A CMR-based Study of Torsional Behavior of Left Ventricle Post-Mitral Valve Repair Surgery

Vahid Naeini[1], Tanmay Mukherjee[1], Seyed Babak Peighambari[1], Emilio A Mendiola[1], Dipan J Shah[2], Reza Avazmohammadi[1]

[1] Department of Biomedical Engineering, Texas A&M University, College Station, TX, USA
[2] DeBakey Heart and Vascular Center, Houston Methodist, Houston, TX, USA

Abstract

Cardiac function is intricately associated with the mechanical dynamics of the left ventricle (LV), particularly its torsional deformation. Mitral valve prolapse (MVP), a prevalent cardiac abnormality, often necessitates surgical repair (MVRe) or replacement (MVRp), which may impact LV torsion and overall cardiac kinematics. This study investigates the changes in LV torsion following MVRe by employing advanced cine cardiac magnetic resonance (CMR) imaging techniques combined with non-rigid image registration to capture and quantify complex three-dimensional myocardial deformations. A small cohort of MVP patients (N=3) was analyzed pre- and post-surgery using an approach that measures in-plane rotations and torsions. This assessment allowed for the characterization of LV torsion across different myocardial transmural depths. Our findings indicated notable alterations in the torsional mechanics post-surgery, particularly in the endocardial layer. These changes suggest that regional torsion, especially within the endocardium, may serve as a useful marker for evaluating the effects of surgical interventions in MVP patients, potentially informing preoperative surgical planning and postoperative care strategies.

1. Introduction

Mitral valve prolapse (MVP) is a structural heart diseases involving mitral valve regurgitation that may require surgical intervention, such as mitral valve repair (MVRe) or replacement (MVRp) [1–3]. These surgeries address critical complications such as flow reflux and reduce the risk of endocarditis. The surgeries are expected to have profound implications on LV hemodynamics, particularly affecting diastolic function. Understanding the biomechanical changes of the myocardium following mitral valve surgery is crucial for mitigating adverse cardiac remodeling and improving patient prognosis [4, 5].

Functional indices based on cardiac kinematics, such as cardiac strain and torsion, have shown promise as valuable metrics of cardiac function that can bridge the gap between tissue-level remodeling and organ-level output. LV torsion, a critical aspect of ventricular dynamics, arises from the orchestrated motion of myocardial fibers, which twist during systole and untwist during diastole. This twisting motion is critical for efficient blood ejection and ventricle filling, reducing the heart's metabolic demands [6–8]. Disruptions in LV torsion dynamics can significantly affect cardiac efficiency and are indicative of underlying cardiac dysfunction [6, 7]. We hypothesize that improved regional torsional behavior in the LV after mitral valve surgery could be associated with improved prognosis and reduced recurrent valvular prolapse.

This study aims to investigate the torsional adaptation of LV post-MVRe. We employed advanced cine cardiac magnetic resonance (CMR) imaging techniques and processed resulting images with a non-rigid image registration (NRIR) algorithm to accurately capture and quantify complex three-dimensional (3D) myocardial deformations [9–11] in a cohort of three patients pre- and post-MVRe. Our findings highlight the significance of LV torsion as a robust biomechanical marker in the assessment of MVP, especially following surgical interventions. The approach seeks to refine diagnostic and therapeutic strategies to optimize recovery and functional outcomes in patients undergoing MVRe and MVRp.

2. Materials and Methods

2.1. Imaging Protocol

Cardiac imaging was conducted on three patients (N=3) diagnosed with MVP pre- and post-MVRe. The research protocol was approved by the Houston Methodist Research Institute review board. Imaging sessions were scheduled for each patient before and 50 days after MVRe surgery. Imaging was performed using a 3.0 Tesla Siemens Ve-

rio MRI scanner with phased-array coils. Standard cine (cMRI) and phase contrast magnetic resonance imaging (PC-MRI) were utilized to capture nine short-axis (SA) slices, each with 20 time frames, throughout one cardiac cycle. The imaging parameters were set as follows: the flip angle varied between 65° and 85°, repetition time was 3.0 ms, echo time was 1.3 ms, spatial resolution ranged from 1.7-2.0 mm by 1.4-1.6 mm, slice thickness was 6 mm with a 4 mm interslice gap, and temporal resolution was set at 35-38 ms. These settings were chosen to ensure detailed visualization of the myocardial structure and motion before and after surgical intervention.

2.2. Image Registration and Analysis

The epicardial and endocardial surfaces of each patient were identified and contoured using Segment v3.0 software. Contours were marked at the end-diastolic (ED) and end-systolic (ES) phases. A non-rigid image registration (NRIR) technique was applied to the segmented images to evaluate myocardial deformation [10, 12]. This technique utilized a convex hull of the segmented contours as a reference to upscale the pixels through interpolation, aiming to reduce the anisotropy of through-plane resolution[13].

The registration algorithm was based on the diffeomorphic demons approach, designed to find the optimal alignment of myocardial structures across different phases of the cardiac cycle by minimizing a predefined cost function. This function includes terms for image similarity, transformation smoothness, and noise robustness, which are critical for accurately mapping and analyzing myocardial deformation [10, 14]. This process allows for a detailed evaluation of myocardial kinematics, which is essential for assessing surgical outcomes.

The cost function used in the registration algorithm is defined as follows:

$$W(\mathbf{c},\mathbf{u}) = \mathbf{1}+\frac{\mathbf{1}}{\sigma_{\mathbf{i}^2}}\|\mathcal{F}-\mathcal{M}\circ\mathbf{c}\|^{\mathbf{2}}+\frac{\mathbf{1}}{\sigma_{\mathbf{x}^2}}\|\mathbf{u}-\mathbf{c}\|^{\mathbf{2}}+\frac{\mathbf{1}}{\sigma_{\mathbf{T}^2}}\|\nabla\mathbf{u}\|^{\mathbf{2}} \tag{1}$$

where σ_i and σ_x represent the noise intensities in the image data and the transformation model, respectively. σ_T is a regularization factor that controls the smoothness of the spatial transformations. The variables $\mathbf{u}$ and $\mathbf{c}$ denote the parametric and non-parametric components of the spatial transformations used to align the images across different cardiac phases. The framework was also employed to compute the Green-Lagrange strain tensor, E, and to reconstruct the left ventricular (LV) geometry through pixel tetrahedralization, enhancing the fidelity of myocardial strain measurements[15].

2.3. Torsion Analysis

The torsional analysis quantified average LV and regional torsion utilizing a moving center of rotation, which was defined by an axis consisting of two centers: one located in the apical section and the other in the basal. These centers were determined as the centers of circles fitted to the endocardial sections of the LV at these respective levels. The fitting of the circles to the endocardial sections was performed using a least-squares approach, minimizing the distance between the points on the endocardial surface and the circle's perimeter. The center $\mathbf{C}$ of the fitted circle for either the apical or basal region was determined by solving:

$$\mathbf{C} = \arg\min_{\mathbf{C}} \sum_{\mathbf{r}\in\mathbf{endo}} \|\mathbf{r}-\mathbf{C}\|^{\mathbf{2}}, \tag{2}$$

where $\mathbf{r}$ represents the position vectors of the endocardial nodes that belong to the endocardial surface. This process identifies the center $\mathbf{C}$ that minimizes the sum of the squared distances between the endocardial points $\mathbf{r}$ and the center $\mathbf{C}$ of the fitted circle for both regions. The centers of these fitted circles, one at the apical and one at the basal section, were used to establish the axis of rotation (AoR, Fig. 1). Vectors were then defined with respect to this AoR to capture the rotational dynamics of the LV. Additionally, to describe the position of points relative to this axis, a polar angle, θ, was introduced such that the angle $\theta = 0^\circ$ was located at the coronal plane.

In-plane rotations were determined by calculating the angle between position vectors at ED and ES, represented by $\mathbf{R_{ED}}$ and $\mathbf{R_{ES}}$, respectively. Thus, the angle of rotation of each pixel was calculated as:

$$\phi = \tan^{-1}\left(\frac{|\mathbf{R_{ED}}\times\mathbf{R_{ES}}|}{\mathbf{R_{ED}}\cdot\mathbf{R_{ES}}}\right) \tag{3}$$

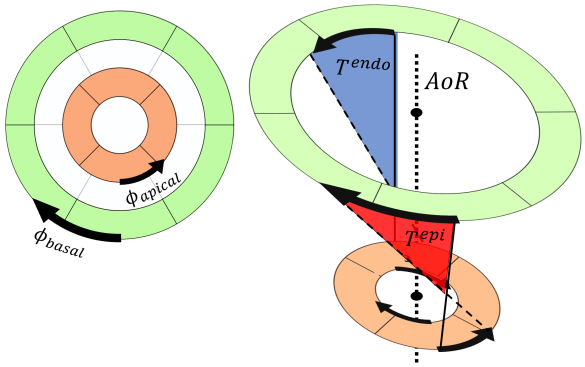

Figure 1: Measuring regional twists ϕ at the basal and apical sections. The diagram shows how T^{endo} and T^{epi} are calculated for specific segments within the left ventricle.

The total torsion of the myocardium was quantified as follows:

$$T = \phi_{apical} - \phi_{basal} \tag{4}$$

where ϕ_{apical} and ϕ_{basal} are the mean angle of rotation of all pixels at the apical and basal, respectively. This torsion measurement characterizes the torsional behavior along the entire length and across the full thickness of the LV. The regional epicardial T^{epi} and endocardial T^{endo} torsion values were calculated as the mean of the pixels on each respective surface between the apical and basal sections. The calculated values for average epicardial torsion are represented as:

$$T^{epi} = \phi^{epi}_{apical} - \phi^{epi}_{basal} \tag{5}$$

where ϕ^{epi}_{apical} and ϕ^{epi}_{basal} represent the mean angle of rotation for points on the epicardial surface at the apical and basal sections. Similarly, endocardial torsion was computed as:

$$T^{endo} = \phi^{endo}_{apical} - \phi^{endo}_{basal} \tag{6}$$

These equations compute the regional torsion between the apical and basal sections on the epicardial and endocardial surfaces, providing a detailed characterization of the torsional behavior across the LV wall.

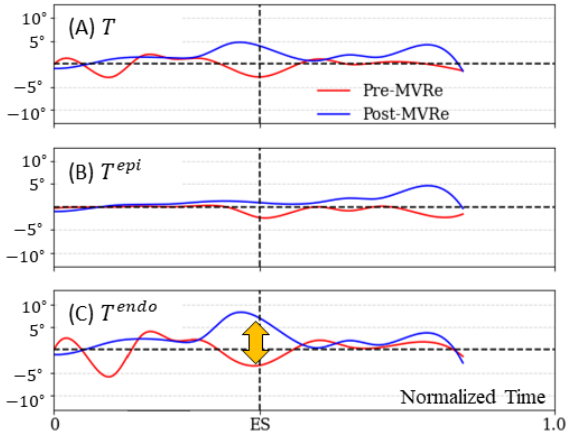

Figure 2: Representative total (**A**) and regional (**B**) epicardial and (**C**) endocardial torsion (n=1) throughout the cardiac cycle before and after mitral valve repair (MVRe). Data correspond to patient #3.

3. Results

Alterations in the total and regional torsional behavior throughout the cardiac cycle were observed following MVRe (Fig. 2). The total torsion of the myocardium generally increased throughout the cardiac cycle, peaking slightly before ES (Fig. 2A). Notably, torsion tended to flip from negative to positive at ES post-MVRe. Minimal torsion was observed in the epicardium pre-MVRe (Fig. 2B) and there was little adaptation observed post-MVRe. In contrast, larger changes in torsion from pre-MVRe to post-MVRe were observed at the endocardial surface of the heart (Figs. 2C, 3), suggesting adaptation at the endocaridum may contribute more to the observed changes in total torsion.

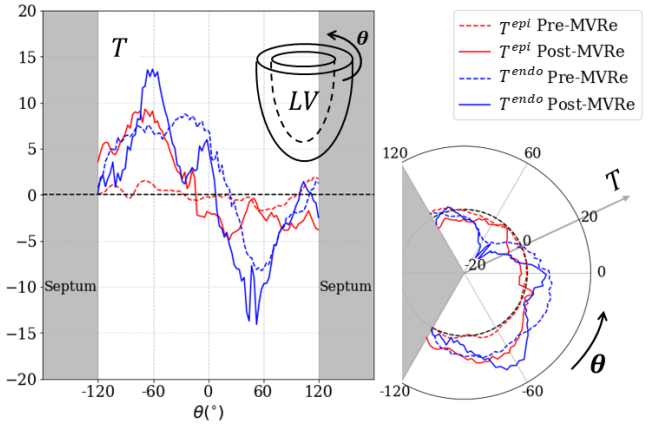

Figure 3: An example of end-systolic pre- and post-surgery torsional behavior in the left ventricle (n=1), representing changes in endocardial (T^{endo}, blue) and epicardial (T^{epi}, red) regional torsion. Data correspond to patient #3.

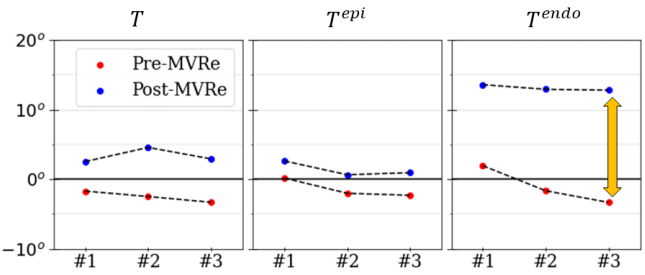

Figure 4: Total and regional epicardial and endocardial torsion for three patients before and after mitral valve surgery. The yellow arrow highlights the changes in endocardial torsion before and after surgery for the same patient shown in Figure 2. Post-surgery trends show notable changes in the endocardium.

At ES, epicardial torsion was near zero in the LV pre-MVRe (Fig. 3), whereas endocardial torsion peaked in the inferior LV at $\theta = \sim 9°$ and transitioned to approximately $\theta = -8°$ at the anterior LV. Both epicardial and endocardial torsion at ES increased in magnitude post-MVRe. The regional distribution of torsion at ES pre- and post-MVRe was maintained; torsion was positive at the inferior region of the LV and negative at the anterior region.

Mean torsion of each patient pre- and post-MVRe indicated similar regional trends in all cases (Fig. 4). Mean

total and regional torsion was negative or near-zero before surgical repair; however, all patients exhibited positive mean total and regional torsion post-MVRe. Similarly, the analysis of mean torsion indicated the largest changes occur at the endocardial surface.

4. Discussion

The findings from this cohort indicate measurable adaptations in LV torsional dynamics following MVRe. Particularly, there was an improvement in counter-rotational torsion post-surgery in all cases. Interestingly, the endocardial layer exhibited more pronounced changes in torsion post-surgery, whereas the epicardial torsion remained relatively stable. This suggests that the endocardium may be more sensitive to the mechanical effects of MVRe, potentially due to altered loading conditions specific to this transmural region. The observed changes suggest a strong link between atrioventricular flow patterns and myocardial kinematics. While our analysis suggests that improvements in mitral valve flow patterns post-surgery lead to changes in LV torsional behavior, the differentiation between acute changes due to immediate improvements post-MVRe from those caused by potential longitudinal remodeling of the LV post-MVRe remains to be explored. Structurally based functional indices, such as strain and torsion, hold promise to aid in prognostication and therapeutic stratification in MVP due to the intrinsic link between LV function and structure. Given the observed adaptations in LV torsional dynamics post-MVRe, a larger longitudinal study is warranted to further explore the link between LV kinematics and cardiac function after mitral valve surgery.

References

[1] Freed LA, Levy D, Levine RA, Larson MG, Evans JC, Fuller DL, Lehman B, Benjamin EJ. Prevalence and clinical outcome of mitral-valve prolapse. New England Journal of Medicine 1999;341(1):1–7.

[2] Guy TS, Hill AC. Mitral valve prolapse. Annual review of medicine 2012;63:277–292.

[3] Castillo JG, Anyanwu AC, Fuster V, Adams DH. A near 100% repair rate for mitral valve prolapse is achievable in a reference center: implications for future guidelines. The Journal of Thoracic and Cardiovascular Surgery 2012; 144(2):308–312.

[4] Lindman BR, Dweck MR, Lancellotti P, Généreux P, Piérard LA, O'Gara PT, Bonow RO. Management of asymptomatic severe aortic stenosis: evolving concepts in timing of valve replacement. Cardiovascular Imaging 2020; 13(2_Part_1):481–493.

[5] Fraldi M, Spadaccio C, Mihos CG, Nappi F. Analysing the reasons of failure of surgical mitral repair approaches—do we need to better think in biomechanics? Journal of Thoracic Disease 2017;9(Suppl 7):S661.

[6] Omar AMS, Vallabhajosyula S, Sengupta PP. Left ventricular twist and torsion: research observations and clinical applications. Circulation Cardiovascular Imaging 2015; 8(6):e003029.

[7] Sengupta PP, Tajik AJ, Chandrasekaran K, Khandheria BK. Twist mechanics of the left ventricle: principles and application. JACC Cardiovascular Imaging 2008;1(3):366–376.

[8] Sengupta PP, Krishnamoorthy VK, Korinek J, Narula J, Vannan MA, Lester SJ, Tajik JA, Seward JB, Khandheria BK, Belohlavek M. Left ventricular form and function revisited: applied translational science to cardiovascular ultrasound imaging. Journal of the American Society of Echocardiography 2007;20(5):539–551.

[9] Avazmohammadi R, Mendiola EA, Soares JS, Li DS, Chen Z, Merchant S, Hsu EW, Vanderslice P, Dixon RA, Sacks MS. A computational cardiac model for the adaptation to pulmonary arterial hypertension in the rat. Annals of Biomedical Engineering 2019;47:138–153.

[10] Mukherjee T, Neelakantan S, Choudhary G, Avazmohammadi R. Improved right ventricular strain estimation in rats using anisotropic diffusion filtering 2023;12470:176–182.

[11] Mendiola EA, da Silva Gonçalves Bos D, Leichter DM, Vang A, Zhang P, Leary OP, Gilbert RJ, Avazmohammadi R, Choudhary G. Right ventricular architectural remodeling and functional adaptation in pulmonary hypertension. Circulation Heart Failure 2023;16(2):e009768.

[12] Mukherjee T, Mendiola EA, Neelakantan S, Shah DJ, Avazmohammadi R. Four-dimensional assessment of left ventricular torsion in mitral valve prolapse using cmr. In Medical Imaging 2024: Image Processing, volume 12926. SPIE, 2024; 108.

[13] Mukherjee T, Keshavarzian M, Fugate EM, Naeini V, Darwish A, Ohayon J, Myers KJ, Shah DJ, Lindquist D, Sadayappan S, et al. Complete spatiotemporal quantification of cardiac motion in mice through enhanced acquisition and super-resolution reconstruction. bioRxiv 2024;2024–05.

[14] Keshavarzian M, Fugate E, Chavan S, Chu V, Arif M, Lindquist D, Sadayappan S, Avazmohammadi R. An image registration framework to estimate 3d myocardial strains from cine cardiac mri in mice 2021;273–284.

[15] Mukherjee T, Usman M, Mehdi RR, Mendiola E, Ohayon J, Lindquist D, Shah D, Sadayappan S, Pettigrew R, Avazmohammadi R. In-silico heart model phantom to validate cardiac strain imaging. Computers in Biology and Medicine 2024;181:109065.

Address for correspondence:

Reza Avazmohammadi,
Department of Biomedical Engineering, Texas A&M University,
101 Bizzell Street,
College Station, TX 77843,
United States, rezaavaz@tamu.edu